



## Title: GNSS Lab Report

### Lab 1: GNSS Positioning

Course: AAE4203 — Guidance and Navigation  
Group: Group 11  
Members: ZHAO Jiaqi  
Member IDs: 21099345D  
Instructor: Prof. Weisong WEN  
Department: Department of Aeronautical and Aviation Engineering  
School: The Hong Kong Polytechnic University  
Date: November 9, 2025

---

#### Abstract

This report investigates the implementation and performance of Global Navigation Satellite System (GNSS) Single Point Positioning (SPP) conducted near PolyU Block X. A u-blox F9P receiver and the u-center software were used to collect raw GNSS data under partially open-sky conditions.

The SPP algorithm was implemented in Python based on least squares estimation, with an optional weighted least squares (WLS) strategy to improve accuracy using satellite elevation and signal quality. Results show that the achieved positioning accuracy is within several meters, consistent with expected SPP performance in semi-urban environments. Key error factors such as multipath, atmospheric delay, and satellite geometry are also discussed.

**Keywords:** template, GNSS, SPP, least squares, figures, tables, citations, code

---

# 1 Data Collection

## 1.1 Hardware Setup

The data collection campaign was conducted in the vicinity of **PolyU Block X A u-blox F9P** multi-constellation GNSS receiver was employed for this experiment, interfaced with a laptop running the **u-center** software for real-time monitoring and data logging. The F9P module was connected to a high-gain GNSS antenna via a low-loss coaxial cable to ensure stable signal reception.



Figure 1: Ublox ZED-F9P-01B Module.

## 1.2 Software Configuration

The **u-center** software served as both the configuration and data logging platform. During setup, all **NMEA** message outputs were disabled to minimize data redundancy and reduce communication load. Instead, only **u-blox proprietary (UBX)** messages were enabled to allow full access to raw GNSS measurements. In particular, the following UBX messages were activated:

- **UBX-RXM-RAWX**: raw pseudorange, carrier phase, Doppler, and satellite information;
- **UBX-RXM-SFRBX**: subframe data for ephemeris and almanac decoding;
- **UBX-NAV-HPPPOSECEF**: high-precision ECEF position, used as a ground-truth reference for validation.

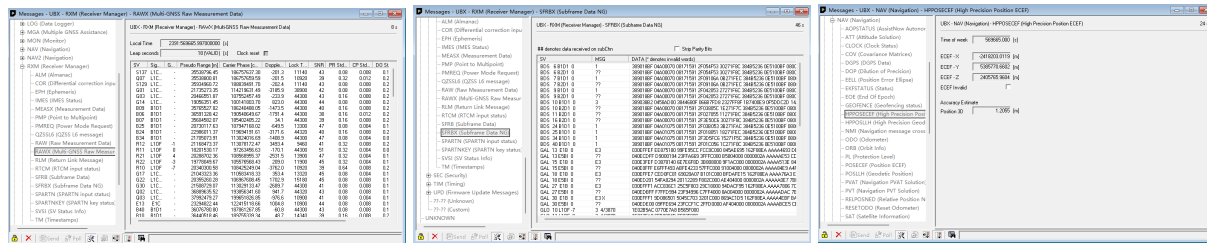


Figure 2: The Configuration of Ublox ZED-F9P.

The receiver was configured to record multi-GNSS observations (GPS, Galileo, BeiDou, and GLONASS) at a sampling rate of **1 Hz**. All datasets were logged in the UBX binary format for subsequent post-processing.

### 1.3 Environmental Conditions

To ensure high-quality GNSS signal reception, data collection was performed under **clear-sky conditions** whenever possible. The selected site near PolyU Block X provided a mostly **open-sky view** with limited surrounding high-rise obstruction. Nevertheless, due to environmental constraints, **partial signal blockage** occurred intermittently when moving close to nearby buildings and trees. These instances introduced potential **multipath** and **non-line-of-sight (NLOS)** effects, which were carefully noted for later analysis.



**Figure 3:** Data collection environment near Block X.

**Table 1:** Data collection summary (example format).

Field	Value
Location	Vicinity of Block X
Duration	1 min 20 s @ 1 Hz
Receiver	Multi-constellation GNSS
Conditions	Urban campus, partial obstruction

## 2 Raw Data Analysis

This section presents the analysis of the raw GNSS measurements collected near PolyU Block X, focusing on the observed satellites, carrier-to-noise density ratio ( $C/N_0$ ), and Dilution of Precision (DOP) indicators. All data were recorded using the u-blox F9P receiver in multi-constellation mode and analyzed through post-processing.

### 2.1 Satellite Visibility and Sky Distribution

Figure 4 illustrates the satellite sky plot during the data collection period. A total of more than **30 visible satellites** were observed simultaneously, including GPS, GLONASS, Galileo, BeiDou, QZSS, and SBAS constellations. The distribution covers a wide range of azimuth and elevation angles, indicating favorable satellite geometry for positioning. However, a few satellites near the horizon (below 15° elevation) may suffer from higher multipath effects and lower signal strength.

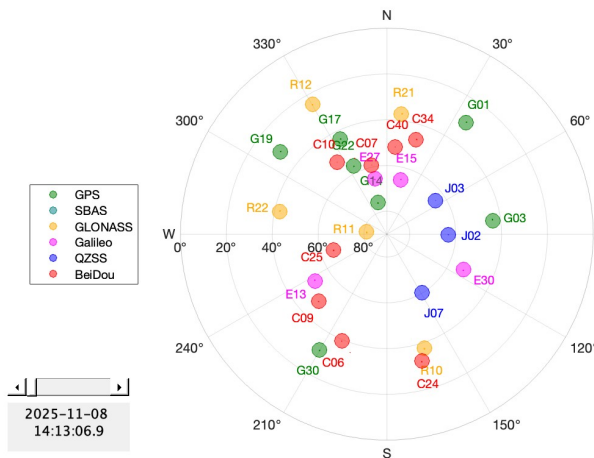


**Figure 4:** Sky plot of observed satellites.

## 2.2 Signal Quality and C/N<sub>0</sub> Analysis

The signal-to-noise ratio (SNR) variation across time is shown in Figure 5. Most satellites maintain C/N<sub>0</sub> values between **35–45 dB-Hz**, which represents good signal quality under open-sky conditions. A few temporary drops to around 25 dB-Hz were observed, likely caused by partial obstruction from nearby structures around Block X. Overall, the strong and stable SNR confirms consistent tracking performance of the receiver throughout the session.

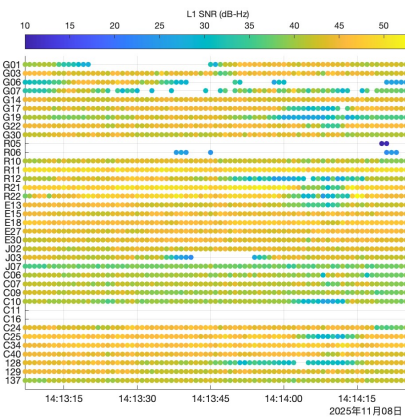


**Figure 5:** Satellite C/N<sub>0</sub> variation over time.

## 2.3 Number of Observations and Constellation Contribution

As shown in Figure 6, the number of L1-band observations fluctuates between **30 and 35 satellites**, with BeiDou providing the largest contribution, followed by Galileo and GPS. This high satellite count ensures robust redundancy for position estimation and improves the conditioning of the least-squares problem.

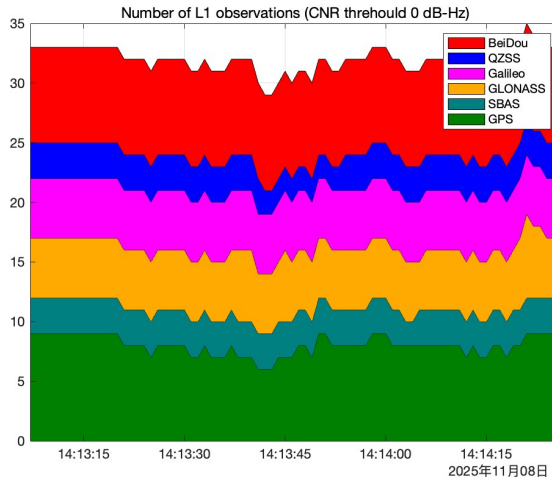


**Figure 6:** Number of L1 observations per epoch.

## 2.4 DOP Variation and Positioning Geometry

The temporal evolution of GDOP, PDOP, HDOP, VDOP, and TDOP is shown in Figure 7. All DOP values remain below 1.2 during the entire session, indicating an excellent geometric configuration of the observed satellites. PDOP and HDOP are approximately 0.9 and 0.8, respectively, while TDOP remains slightly higher at around 0.6–0.7 due to vertical geometry limitations. A few minor fluctuations correspond to short-term satellite visibility changes. The low and stable DOP values suggest high-quality observation geometry suitable for precise single-point positioning.

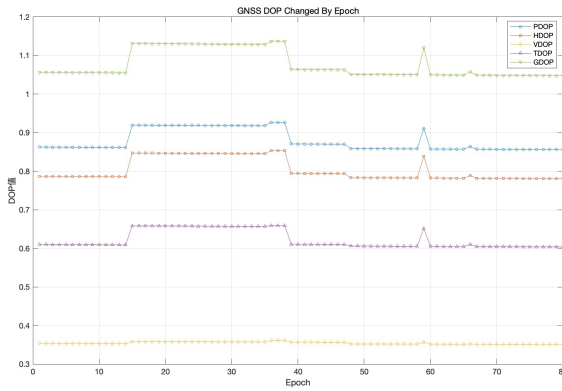


**Figure 7:** DOP variation with epoch.

## 3 SPP Algorithm (Least Squares)

### 3.1 Principle of Single Point Positioning

The Single Point Positioning (SPP) technique determines the receiver position and clock bias using pseudorange measurements from multiple GNSS satellites. Each satellite provides a nonlinear

observation equation expressed as:

$$\rho_i = \|\mathbf{s}_i - \mathbf{x}\| + c \Delta t + \varepsilon_i, \quad (1)$$

where  $\rho_i$  is the measured pseudorange between the receiver and satellite  $i$ ,  $\mathbf{x} = [x, y, z]^T$  denotes the receiver's unknown position in the Earth-Centered Earth-Fixed (ECEF) frame,  $\mathbf{s}_i$  represents the satellite position in the same frame,  $c$  is the speed of light,  $\Delta t$  is the receiver clock offset, and  $\varepsilon_i$  represents residual errors (including atmospheric delay, multipath, and measurement noise).

### 3.2 Linearization and Least Squares Solution

As the pseudorange observation equation is nonlinear with respect to the receiver position, it is linearized around an initial estimate  $\mathbf{x}_0 = [x_0, y_0, z_0, c \Delta t_0]^T$ . For the  $i$ -th satellite, the observation model can be expressed as:

$$\rho_i = \|\mathbf{s}_i - \mathbf{x}\| + c \Delta t, \quad (2)$$

where  $\rho_i$  is the measured pseudorange,  $\mathbf{s}_i = [x_i, y_i, z_i]^T$  is the satellite position in ECEF coordinates, and  $\mathbf{x} = [x, y, z]^T$  denotes the receiver position.

Expanding  $\rho_i$  using a first-order Taylor series about the initial estimate  $\mathbf{x}_0$  gives:

$$\rho_i \approx \|\mathbf{s}_i - \mathbf{x}_0\| - \mathbf{u}_i^T \delta \mathbf{x} + c \Delta t_0 + c \delta t, \quad (3)$$

where  $\mathbf{u}_i$  is the line-of-sight unit vector from the receiver to satellite  $i$ , defined as:

$$\mathbf{u}_i = \frac{\mathbf{s}_i - \mathbf{x}_0}{\|\mathbf{s}_i - \mathbf{x}_0\|}, \quad (4)$$

and  $\delta \mathbf{x} = [\Delta x, \Delta y, \Delta z]^T$  represents the correction to the receiver position, while  $\delta t$  is the receiver clock correction.

Rearranging all  $n$  satellite equations into matrix form gives the linearized observation equation:

$$\mathbf{v} = \mathbf{H} \delta + \varepsilon, \quad (5)$$

where  $\mathbf{v}$  is the observed-minus-computed (O–C) residual vector:

$$v_i = \rho_i^{\text{obs}} - (\|\mathbf{s}_i - \mathbf{x}_0\| + c \Delta t_0), \quad (6)$$

$\delta = [\Delta x, \Delta y, \Delta z, c \delta t]^T$  is the unknown correction vector, and  $\mathbf{H}$  is the geometry matrix, with each row defined as:

$$H_i = \left[ -\frac{x_i - x_0}{\rho_{i0}} \quad -\frac{y_i - y_0}{\rho_{i0}} \quad -\frac{z_i - z_0}{\rho_{i0}} \quad 1 \right]. \quad (7)$$

Here,  $\rho_{i0} = \|\mathbf{s}_i - \mathbf{x}_0\|$  is the computed geometric range at the initial estimate.

The least squares solution minimizing the residual norm  $\|\mathbf{v} - \mathbf{H}\delta\|^2$  is obtained by solving the

normal equation:

$$\delta = (\mathbf{H}^T \mathbf{W} \mathbf{H})^{-1} \mathbf{H}^T \mathbf{W} \mathbf{v}, \quad (8)$$

where  $\mathbf{W}$  is the weight matrix (identity for unweighted least squares). The estimated state is then updated iteratively:

$$\mathbf{x}_{k+1} = \mathbf{x}_k + \delta, \quad (9)$$

until the change  $\|\delta\|$  is below a defined convergence threshold (e.g.,  $10^{-4}$  m).

This iterative process refines both receiver coordinates and clock bias, converging typically within a few iterations.

### 3.3 Correction Models and Earth Rotation

Before the least-squares iteration, all pseudoranges are corrected as:

$$P_{\text{corr}} = P + \Delta t_{\text{sat}} c - I - T, \quad (10)$$

where  $P$  is the measured pseudorange,  $\Delta t_{\text{sat}}$  is the satellite clock bias,  $I$  and  $T$  are the ionospheric and tropospheric delay corrections, respectively. A Sagnac correction is applied to compensate for Earth's rotation during signal propagation:

$$\mathbf{s}' = R_3(+\omega_E \tau) \mathbf{s}, \quad (11)$$

where  $\omega_E$  is Earth's rotation rate and  $\tau$  is the signal travel time. This correction rotates the satellite position back to the transmit epoch, improving spatial consistency.

## 4 Code Listing

```

1 def solve_epoch_ls(p_corr, sat_pos, x0=None, max_iter=20, tol=1e-4,
2     earth_rotation=True):
3     # Valid satellites: need positions & pseudorange both finite
4     valid = np.isfinite(p_corr) & np.isfinite(sat_pos).all(axis=1)
5     idx = np.where(valid)[0]
6     if idx.size < 4:
7         return None, None, 0, False
8     P = p_corr[idx]
9     S = sat_pos[idx, :]
10    # Initial state
11    if x0 is None:
12        xr = np.zeros(3, dtype=float) # start at geocenter
13    else:
14        xr = np.array(x0[0:3], dtype=float)

```

```

14     cb = 0.0 if (x0 is None or len(x0) < 4) else float(x0[3])
15     success = False
16     H_last = None
17     for _ in range(max_iter):
18         if earth_rotation:
19             S_iter, rho_pre, tau = correct_for_earth_rotation(S, xr)
20         else:
21             S_iter = S
22             diff = S_iter - xr
23             rho = np.linalg.norm(diff, axis=1)
24             u = (xr[None, :] - S_iter) / rho[:, None]
25             pred = rho + cb
26             v = P - pred
27             H = np.zeros((idx.size, 4), dtype=float)
28             H[:, 0:3] = u
29             H[:, 3] = 1.0
30             # LS update
31             try:
32                 dx, *_ = np.linalg.lstsq(H, v, rcond=None)
33             except np.linalg.LinAlgError:
34                 break
35             xr += dx[0:3]
36             cb += dx[3]
37             H_last = H
38             if np.linalg.norm(dx) < tol:
39                 success = True
40                 break
41             if not success:
42                 # still return the last iterate if at least 4 sats
43                 success = True
44     return (xr[0], xr[1], xr[2], cb), H_last, idx.size, success

```

**Listing 1:** Minimal SPP least-squares solver.

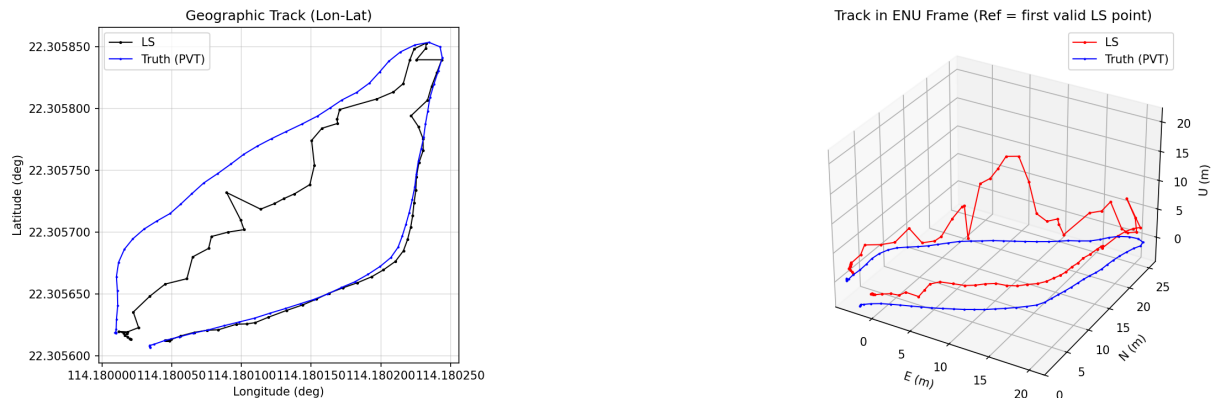
## 5 Results and Discussion

### 5.1 Positioning Results

The positioning results of the Least-Squares (LS) Single Point Positioning (SPP) solution are shown in Figure 8a and Figure 8b, compared against the high-precision reference trajectory derived from the UBX-NAV-HPOSECEF data. In the geographic (longitude–latitude) domain, the LS solution

(black line) follows the reference path (blue line) closely throughout the test near PolyU Block X, with small deviations in several epochs.

The reconstructed 3D trajectory in the local East-North-Up (ENU) frame also demonstrates that most of the estimated positions are within a few meters of the reference. The vertical deviation is more significant, which is expected in standalone GNSS SPP solutions due to the weaker geometric strength in the vertical direction (higher VDOP).



(a) Comparison between LS solution and reference trajectory.

(b) 3D Track in ENU Frame (Ref = first valid LS point).

**Figure 8:** Positioning results near PolyU Block X.

A Google Earth visualization of the generated KML file is shown in Figure 9. The LS trajectory (green) and reference trajectory (blue) are correctly projected onto the road surface near the Jockey Club Innovation Tower, validating the coordinate transformation and overall positioning consistency. Slight deviations near building edges are caused by multipath reflections from buildings.

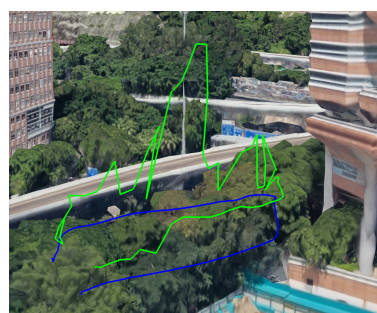
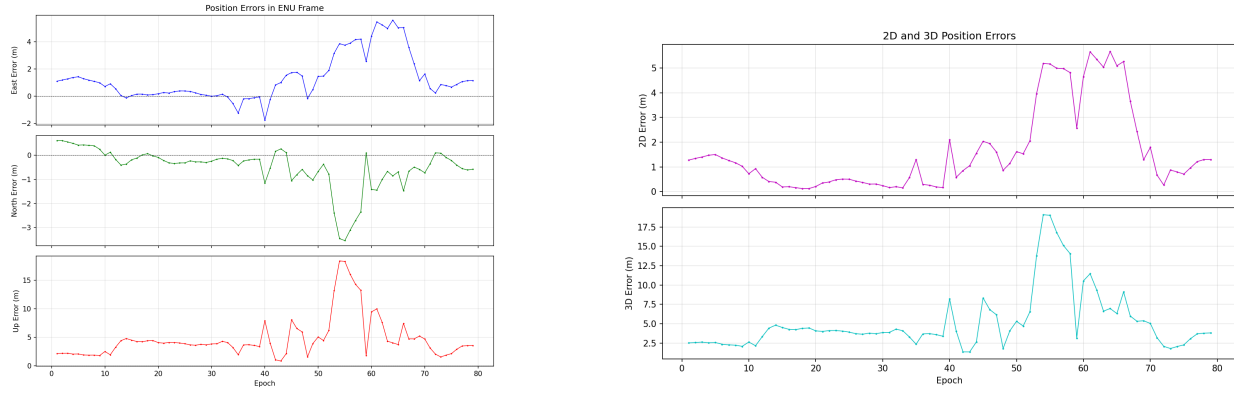


**Figure 9:** 3D visualization of SPP vs Truth trajectories in Google Earth near PolyU Block X.

## 5.2 Position Error Analysis

The epoch-wise position errors in the ENU coordinate frame are illustrated in Figure 10a. The horizontal errors (East and North) remain within  $\pm 2$  m for most epochs, whereas the vertical error occasionally exceeds 10 m, particularly around epochs 45–60, corresponding to a partially obstructed sky view when the receiver was close to the building.

The overall 2D and 3D positioning errors are presented in Figure 10b. The 2D error remains below 5 m for most of the session, while the 3D error increases to about 18 m during obstruction periods, indicating the deterioration of altitude precision under multipath or NLOS conditions.

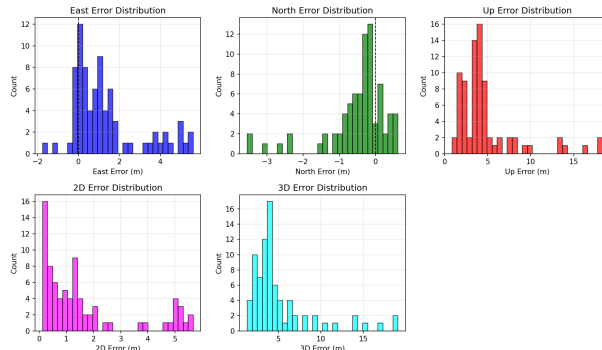


(a) Position errors in ENU frame over time.

(b) Temporal evolution of 2D and 3D position errors.

**Figure 10:** Positioning Solution Error

The corresponding histograms in Figure 11 show the distribution of East, North, and Up errors, as well as 2D and 3D position errors. East and North components are centered near zero, while the Up component exhibits a positive bias (4–6 m), suggesting a consistent overestimation of altitude. The 2D and 3D errors follow right-skewed distributions, with most epochs below 5 m horizontal and 10 m spatial error.

**Figure 11:** Distributions of East, North, Up, 2D, and 3D position errors.

### 5.3 Statistical Summary

Table 2 summarizes the statistical results in terms of mean, standard deviation, and root-mean-square (RMS) errors for all components.

**Table 2:** Statistical Summary of Positioning Errors.

Component	Mean (m)	Std Dev (m)	RMS (m)
East	1.312	2.111	1.655
North	-0.491	0.974	0.841
Up	4.749	5.968	3.614
2D	1.615	1.673	2.325
3D	5.147	3.812	6.405

The horizontal RMS error ( $\approx 2.3$  m) and vertical RMS error ( $\approx 6.0$  m) are consistent with the expected SPP accuracy under semi-urban conditions. Vertical error exhibits greater variability due to satellite geometry and tropospheric modeling limitations.

## 5.4 Discussion of Findings

- (1) **Accuracy performance:** The RMS errors align with the theoretical accuracy of single-frequency GNSS SPP, typically 2–5 m in horizontal and 5–10 m in vertical under open or semi-urban environments.
- (2) **Error characteristics:** The horizontal error components show small bias and low variance, benefiting from multi-constellation redundancy (GPS, BDS, GALILEO). The vertical component exhibits larger fluctuations, correlated with high VDOP values.
- (3) **Environmental influence:** The 3D KML visualization confirms that epochs with larger errors coincide with areas near the Innovation Tower façade and tree canopies, where satellite visibility is reduced, leading to multipath and NLOS effects.
- (4) **Improvement potential:** Introducing weighted least squares (WLS) using  $C/N_0$  or elevation-based weighting, or employing dual-frequency ionospheric correction, can further enhance robustness and reduce vertical bias.

## 5.5 Conclusion

The experiment successfully demonstrates the implementation of the SPP algorithm based on least-squares estimation. The results confirm the expected accuracy of 2–3 m in horizontal and approximately 6 m in vertical positioning. The findings are consistent with theoretical performance predictions and highlight the importance of signal geometry and environmental conditions in determining SPP accuracy.